

Computers and Electronics in Agriculture

Manuscript Details

Manuscript number	COMPAG_2019_1895_R2
Title	MHW-PD: a robust rice panicles counting algorithm based on deep learning and multi-scale hybrid window
Article type	Research Paper

Abstract

In-field assessment of rice panicle yields accurately and automatically has been one of the key ways to realize high-throughput rice breeding in the modern smart farming. However, practical rice fields normally consist of many different, often very small sizes of panicles, particularly when large numbers of panicles are captured in the imagery. In these cases, the integrity of panicle feature is difficult to extract due to the limited panicle original information and substantial clutters caused by heavily compacted leaves and stems, which results in poor counting efficacy. In this paper, we propose a simple, yet effective method termed as Multi-Scale Hybrid Window Panicle Detect (MHW-PD), which allows the identification and counting of rice panicles robustly independent of the panicle number (density) in the scene. On the basis of quantifying and analyzing the relationship among the receptive field, the size of input image and the average dimensions of panicles, the MHW-PD gives dynamic strategies for choosing the appropriate feature learning network and constructing adaptive multi-scale hybrid window (MHW), which maximizes the richness of panicle feature. Besides, a fusion algorithm is involved to remove the repeated counting of the broken panicles to get the final panicle number. With extensive experimental results, the MHW-PD has achieved ~87% of panicle counting accuracy; and the counting accuracy just decreases by ~8% when the number of panicles per image increases from 0 to 80, which shows better in stability than all the competing methods adopted in this work. The MHW-PD is demonstrated qualitatively and quantitatively that is able to deal with high density of panicles.

Keywords	Rice; Panicle counting; Deep learning; Multi-Scale Hybrid window; Faster-RCNN;
Corresponding Author	Haiyan Jiang
Corresponding Author's Institution	Nanjing Agricultural University
Order of Authors	Xu Can, Haiyan Jiang, Peter Yuen, Zaki Zaki, Chen Yao

Highlights

- (1) A counting algorithm is developed for in-field rice panicles with high density.
- (2) The appropriate CNN is chosen by analyzing receptive field and panicle size.
- (3) A MHW is calculated quantitatively to maximize the richness of panicle feature.
- (4) A fusion module is involved to remove the repeated counting of broken panicle.
- (5) Stability and robustness of MHW-PD is demonstrated by several experiments.

1 ***MHW-PD: a robust rice panicles counting algorithm based on***
2 ***deep learning and multi-scale hybrid window***

3 ***Xu Can¹, Jiang Haiyan^{1,2*}, Peter Yuen³, Zaki Ahmad Khan¹, Chen Yao¹***

4 ***1 College of Information science & Technology, Nanjing Agricultural University***

5 ***Nanjing 210095, Jiangsu, China***

6 ***2 National Engineering & Technology Center for Information Agricultural,***

7 ***Nanjing Agricultural University Nanjing 210095, Jiangsu, China***

8 ***3 Electro-Optics & Remote Sensing, Centre for Electronics Warfare, Information &***

9 ***Cyber (CEWIC), Cranfield University, Swindon, U.K***

10 **Abstract**

11 In-field assessment of rice panicle yields accurately and automatically has been one of
12 the key ways to realize high-throughput rice breeding in the modern smart farming.
13 However, practical rice fields normally consist of many different, often very small
14 sizes of panicles, particularly when large numbers of panicles are captured in the
15 imagery. In these cases, the integrity of panicle feature is difficult to extract due to the
16 limited panicle original information and substantial clutters caused by heavily
17 compacted leaves and stems, which results in poor counting efficacy. In this paper, we
18 propose a simple, yet effective method termed as Multi-Scale Hybrid Window Panicle
19 Detect (MHW-PD), which focuses on enhance the panicle features to detect and count
20 the large number of small-sized rice panicles in the in-field scene. On the basis of

quantifying and analyzing the relationship among the receptive field, the size of input image and the average dimensions of panicles, the MHW-PD gives dynamic strategies for choosing the appropriate feature learning network and constructing adaptive multi-scale hybrid window (MHW), which maximizes the richness of panicle feature. Besides, a fusion algorithm is involved to remove the repeated counting of the broken panicles to get the final panicle number. With extensive experimental results, the MHW-PD has achieved ~87% of panicle counting accuracy; and the counting accuracy just decreases by ~8% when the number of panicles per image increases from 0 to 80, which shows better in stability than all the competing methods adopted in this work. The MHW-PD is demonstrated qualitatively and quantitatively that is able to deal with high density of panicles.

Keywords : Rice; Panicle counting; Deep learning; Multi-Scale Hybrid window; Faster-RCNN;

1 Introduction

The main diet of the population in Asia is predominately rice, thus the monitoring of rice yield accurately is crucially important to the growers for the prediction of harvest and the development of strategic growth plan. The yield of cereal crops, such as rice, is largely determined by three agronomic indicators: the kernel number, the seed setting rate and the 1000-grain weight(Slafer et al., 2014). Previous researches (Ferrante et al., 2017; Jin et al., 2017)have shown that the number of kernels per unit area is the most relevant agronomic traits to grain yield. However, this number of

grains per unit area not only relates to the seed setting rate, but also it is strongly dependent on the number of panicle per unit area. Therefore, it is desirable for the breeders to obtain the number of panicles per unit area quickly and accurately. At present, this is often achieved through counting manually in most rice cultivation or breeding research, which costs huge amount of time and labor. Furthermore, due to the great morphological similarity between different plants in the field, and also the subjectivity in individual observers, it is very error-prone for counting rice panicles manually particularly in large-scale production scenarios. Therefore, a fast and relatively accurate automatic counting method is needed: for both production as well as scientific research needs such as phenotyping work.

Automatic counting method based on machine vision technology is considered to be an effective alternative to manual counting, and successful precedents such as the counting of plant leaves(Aich et al., 2017; Barré et al., 2017; Dobrescu et al., 2017; Giuffrida et al., 2016) and fruits(Maldonado Jr et al., 2016; Mussadiq et al., 2015; Stein et al., 2016) have been reported. The effectiveness of this automatic counting method is heavily dependent on the ability of the machine to recognize the targets. In terms of automatic counting of rice panicles, the existing panicle recognition methods can be divided into two main categories: the segmentation technique which bases on colour and/or textural features and the candidate region-based classification methods. Panicle segmentation method (Cointault et al., 2008; Pound et al., 2017) extracts the colour or texture of the panicle, and the rice panicles are segmented from the

63 background before they are counted. Zhou et al. (Zhou et al., 2018) employed
64 principal component analysis to extract representative features of wheat from RGB
65 images such as colour, texture and edge for wheat panicle segmentation, and ~80% of
66 count accuracy by using a trained dual support vector machine has been reported.
67 Fernandez et al.(Fernandez-Gallego et al., 2018) proposed a fast low-cost wheat
68 panicle segmentation algorithm which uses Laplacian, Median and Maxima (LMM)
69 filters to remove clutter backgrounds and had achieved good panicle counting results.
70 The panicle segmentation method is of a low computational complexity algorithm but
71 the result is sensitive to the illumination conditions of the imagery data (Guo et al.,
72 2015).

73 The candidate region classification is the method that clusters features over the
74 spatial domain. The key of the algorithm is the generation of candidate regions,
75 through features such as color or texture and the candidate regions are subsequently
76 formed by using the hysteresis threshold of the I2 color plane (Duan et al., 2015) and
77 the Laws texture energy over the input image(Qiongyan et al., 2017). This method
78 eliminates more of the clutter background than that of the segmentation approach,
79 hence it achieves better counting accuracy to some extents. Alternative approach that
80 utilizes superpixel technique for improving the quality of the candidate region
81 generation through better preservation of boundary information and to reduce
82 boundary adhesions, has been widely explored(Lu et al., 2016). Some authors
83 employed simple linear iterative clustering for the generation of superpixel and then

classified the region candidates using convolutional neural network (Xiong et al., 2017) or classifier trained based on colour feature(Du et al., 2019). Further study using more effective segmentation method that utilize superpixel in different scales and couple with a trained linear regression model for counting different varieties of rice panicles has also been reported(Olsen et al., 2018).

The recent work had made the better use of the powerful feature learning capabilities of the CNN (Convolutional Neural Network, CNN). More sophisticated feature learning that utilizes a full convolution network for counting field wheat spikelet have reported a counting accuracy of about 86%(Alkhudaydi et al., 2019). Other method(Hasan et al., 2018) used the R-CNN(Girshick et al., 2014) for wheat panicle identification counting, for the object detection algorithm focus on solving the composite problem of classification and localization. The latest work(Madec et al., 2019) introduced the Faster-RCNN(Ren et al., 2015) method into wheat panicle counting and got a 91% counting accuracy. For the rice panicles we focus on, they will droop due to their self-weight on the maturity-stage, which means the crowded panicles cram together with leaves and even occluded by leaves locally. Meanwhile, the size of the panicles in the image tends to reduce when high density of panicles, e.g. >50 panicles/image, is captured by the camera. In this case, the very limited information (color/textural/spatial) of the panicle, which is embedded closely in substantial amount of clutter background, greatly reduces the feature learning efficiency of the existing object detection algorithms(He et al., 2015; Liu et al., 2016;

Redmon et al., 2016; Redmon et al., 2017) and inevitably resulting in large counting error. Thus, there is a real need to develop a new auto approach to allow a rapid counting of the scene with large number of small-sized rice panicles per image.

2 Principles and designs of the MHW-PD for panicle counting

2.1 Analysis of application of Faster-RCNN

Faster-RCNN is one of the representative detection algorithms based on regions(Han et al., 2018), which features the strengths of algorithmic structures like that of the RCNN(Girshick et al., 2014), the SPP-Net(He et al., 2015) and the Fast-RCNN (Girshick, 2015). As shown in Figure 1, Faster-RCNN has capabilities such as feature learning, candidate region generation, target classification and positional frame generation. When Faster-RCNN learns feature based on a CNN, one important point is the receptive field, which is defined by the region in the input space that corresponds to any pixel on a particular CNN's feature map. In the circumstances when train a model to make classification and location, the receptive field of every position on the feature map have to span over all the anchors that the target/object represents. Otherwise the feature vectors of the anchors will not have enough information to make predictions, leading some objects missed by detection model. This is particular true when the target in question is relatively small in physical size in comparison to that of the background objects, for example, the small-sized rice panicles here in our scenario.

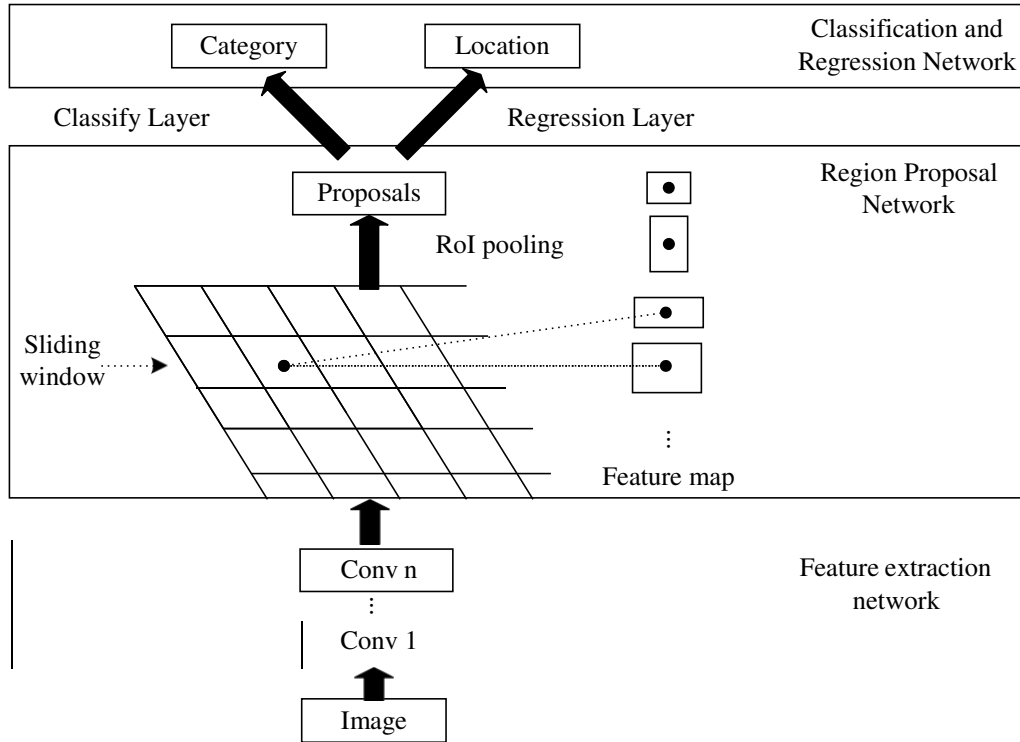


Fig. 1 Outlines the schematic layout of the Faster-RCNN network

125 2.2 Overall design of the MHW-PD

126 The objective of the paper is to report an adaptive multi-scale hybrid window
 127 (MHW) pre-processing technique to enhance the signal to noise ratio of the panicle
 128 features in the input image, and to couple it with Faster-RCNN network to achieve
 129 robust counting accuracy for the large number of small-sized panicles in image. For
 130 the problem of information loss in the process of learning small-sized panicles
 131 feature, we firstly designed a dynamic mechanism for selecting feature learning
 132 network, which is based on the relationship between the size of the rice panicle and
 133 the dimension of the receptive field. Secondly, we dynamically calculated the hybrid
 134 windows in different scales by partitioning the image into subsections by quantifying
 135 the relationship between the input image size and the feature learning network

parameters. This helps to reduce the background complexity by suppressing the clutter background particularly when the number of rice panicles increases. The framework of MHW-PD (Figure 2) consists of the following work flow: a) select feature learning network dynamically; b) calculate the structure of the hybrid windows; c) train the automatic rice panicle counting model based on the Faster-RCNN; d) fuse the same rice panicle which has been partitioned into several entities to remove the multiple counting; e) output the final number of rice panicles count of the test image.

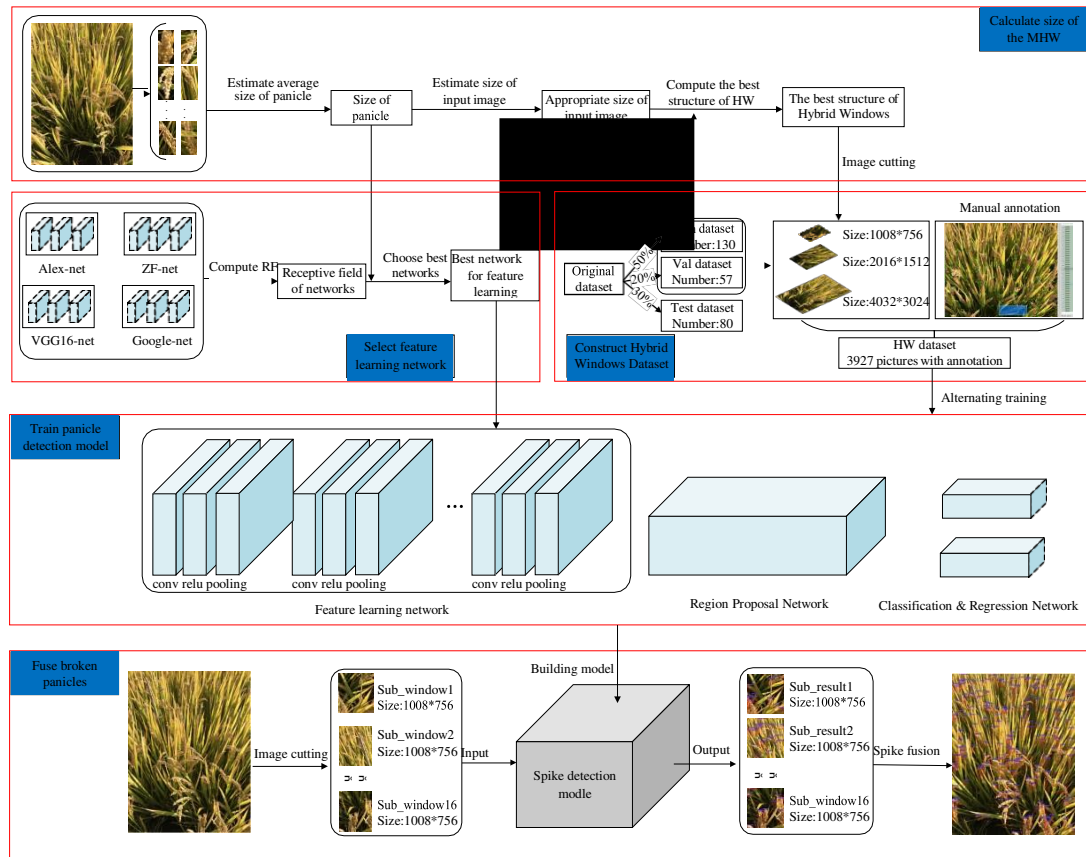


Fig. 2 The schematic layout of the MHW-PD for the robust detection and counting of rice panicles

2.2.1 Selection of the feature learning network

Feature learning is the technique that iteratively abstracts the semantic and position information of the target from the image data and converts them into feature

maps. The extracted features are dependent on the layer property and thus the receptive field of a layer can be given by equation (1) (Ren et al., 2018).

$$S_R(t) = (S_{RF}(t-1) - 1)N_s(t) + S_f(t) \quad (1)$$

Where $S_{RF}(t)$ and $N_s(t)$ are the receptive field size and the step size of the t^{th} convolution layer, and $S_f(t)$ is the size of filter of the t^{th} convolution layer. The ideal dimension of the receptive field is a delicate balance between clutter noise and the integrity of the extracted feature. In the present Faster-RCNN experiment, the relationship between the receptive field of the feature learning network and the object/target has been set as in equation (2):

$$\frac{S_{RF}(t)}{S_{obj}(h_{obj}, w_{obj})} \approx 1 \quad (2)$$

Where $S_{obj}(h_{obj}, w_{obj})$ represents the size of the object to be detected, and h_{obj} and w_{obj} respectively represent the length and width of the minimum circumscribed rectangle of the target to be detected. According to equation (2), the ideal dimension of the receptive field is ideally to be about the same as that of the targets (i.e. the rice panicles). According to equation (1), the dimensions of the receptive field of the last convolutional layer of the most popular networks, such as the Alex-Net(Krizhevsky et al., 2012), ZF-Net(Zeiler et al., 2014), VGG16-Net(Simonyan et al., 2014) and Google-Net (Szegedy et al., 2015) are tabulated in Table 1. The average sizes (length \times width) of rice panicles in the image data that have been selected for this work is about 260 \times 180 pixels. Thus the VGG16 network which features a receptive field of 212 \times 212 may present a closer match to the average panicle dimensions of the data

that utilized in this work than other networks. Therefore, the VGG16 network and the classification layer have been selected as the feature learning network in this work.

Table 1. Tabulated the receptive field of different nets for the 800×600 pixels input image

Net name	Reception field of the last layers	S_{RF}/S_{obj}
ZF-Net	139×139	0.41
Alex-Net	195×195	0.81
VGG16-Net	212×212	0.96
Google-Net	224×224	1.07

2.2.2 Design of the Multi-scale Hybrid Window (MHW) Structure

Targets are generally regarded as small when they are less than 32×32 pixels or when their length and width are smaller than a tenth of that of the image where they are contained. The construction of a multi-scale hybrid window by partitioning a picture into sub-images will tend to enhance the proportions of the object features with respected to the background within the sub-image, especially when the objects are small. The richer of the target feature will enhance the discrimination ability of the RPN to identify/propose the anchors to be foreground or background thereby improving the detection efficiency. The design of the MHW structure involves the considerations of: i) the various sizes of hybrid windows needed for a given input image, ii) the number of window layers and iii) the selection of layers that are the most suitable to the ranges of various input image sizes.

The largest hybrid window that can theoretically be constructed in each layer of the n-layer feature learning network can be given by equation (3):

$$\begin{cases} A_{H(t)} = \frac{H + S(t) + 2 * S_p(t)}{N_s(t)} + 1 \\ A_{W(t)} = \frac{W + S(t) + 2 * S_p(t)}{N_s(t)} + 1 \end{cases} \quad t = 1, 2, \dots, n \quad (3)$$

186 Where $A_{H(t)}$ and $A_{W(t)}$ represent the length and width of the t^{th} feature map of the
 187 feature learning network respectively, H and W represent the length and width of
 188 the original raw image respectively, and n is maximum number of layers in the
 189 feature learning network. $N_s(t)$ is the step size of the t^{th} convolution layer, and S_f
 190 (t) is the size of the filter of t^{th} convolution layer, and $S_p(t)$ is the expansion of
 191 the t^{th} convolution layer. The optimal input image size is given in equation (4):

$$192 \quad \begin{cases} h_{in} = \frac{h_{obj}}{T_1} & 0.1 < T_1 < 1 \\ w_{in} = \frac{w_{obj}}{T_2} & 0.1 < T_2 < 1 \end{cases} \quad (4)$$

193 where h_{in} and w_{in} represent the length and width of the optimum input image
 194 dimensions; h_{obj} and w_{obj} represent the length and width of the smallest rectangle
 195 of the object to be detected respectively; T_1 and T_2 represent the ratio of the length
 196 and width of the object respected to the dimensions of the input image respectively.
 197 The optimal dimensions of the multi-scale hybrid window structure can then be
 198 deduced as shown in equation (5):

$$199 \quad \begin{cases} h_{HW}(i) = A_{H(t)} & A_{H(t)} \in (h_{min}, h_{max}) \\ w_{HW}(i) = A_{W(t)} & A_{W(t)} \in (w_{min}, w_{max}) \end{cases} \quad i = 1, 2, \dots, p \text{ \& } t = 1, 2, \dots, n \quad (5)$$

200 When there are p layers of multi-scale hybrid windows, $h_{HW}(i)$ and $w_{HW}(i)$
 201 represent the optimal length and width of the i^{th} layer respectively; (h_{min}, h_{max}) and
 202 (w_{min}, w_{max}) represent the possible range of the optimal length and width of the input

203 images that will produce the best learning and classification performances.

204 **2.2.3 MHW fusion**

205 One of the drawbacks for partitioning the input image into sub-images is the

206 panicle may be unintentionally cut into several parts in different sub-images. To
 207 eliminate the repeated counting of the same panicle that resides in various sub-images
 208 during the prediction stage, a fusion algorithm is designed to detect the occurrence of
 209 the panicle that has been subdivided into parts. A simple way to correct this
 210 unintentional partition of the target object is to check the vicinity of all the predicted
 211 boxes. A simple spatial distance monitor algorithm has been implemented to check
 212 the vicinity of all the predicted location boxes: if two predicted boxes are adjacent or
 213 very close to each other while their sum of size (height \times length) is close to the
 214 average panicle size, e.g. when they are say <10 pixels apart and sum is between
 215 130 \times 90 pixels and 390 \times 270 pixels (from 1/2 to the 3/2 of the average panicle size),
 216 the boxes pairs will be merged into one by adopting the largest vertices of the corner
 217 coordinate as illustrate in Table 2 and Figure 3.

218 **Table 2. The Mini-Code of the Fusion Algorithm for recombining dissected rice panicles**

Input: $(x1_n, y1_n, x2_n, y2_n)$: the coordinates of the left upper and right lower vertices of the panicle detected in
 sub-windows
Output: $(x1'_m, y1'_m, x2'_m, y2'_m)$: the coordinates of prediction boxes fused
For ($k = 1; k \leq n; k++$)
 For ($t = 1; t \leq n; t++$)
 If ($|x1_k - x2_t| < 10 \ \&\& \ |y1_k - y2_t| < 2h$) \parallel ($|y1_k - y2_t| < 10 \ \&\& \ |x1_k - x2_t| < 2w$) \parallel
 ($90 < (|y1_k - y2_k| + |y1_t - y2_t|) < 270$) \parallel ($130 < (|x1_k - x2_k| + |x1_t - x2_t|) < 390$)
 $(x1'_m, y1'_m, x2'_m, y2'_m) = (\min(x1_k, x1_t), \min(y1_k, y1_t), \max(x2_k, x2_t), \max(y2_k, y2_t))$
 $m++;$

219

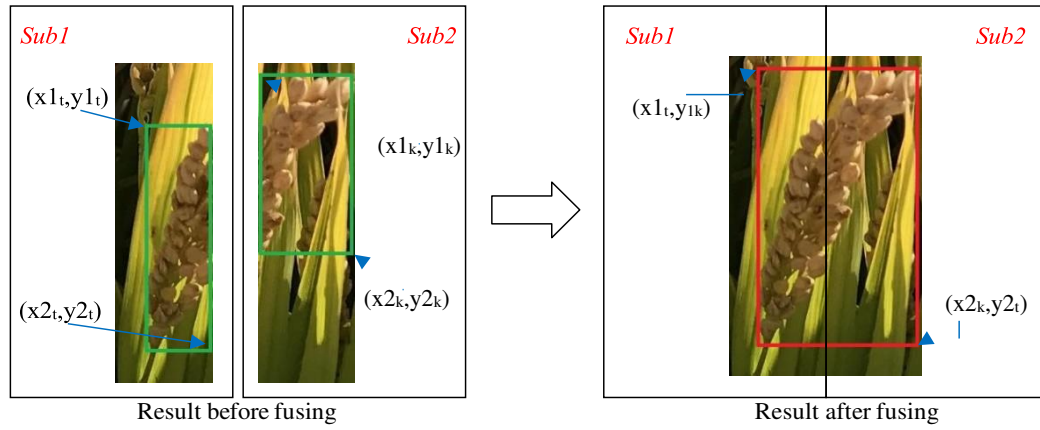


Fig. 3 Illustrated the fusion of vertically dissected rice panicles

220 3 Construction of dataset and model

221 3.1 Image data acquisition

222 The rice variety chosen is ‘Nanjing46’ and all images were acquired in Nanjing,
 223 Jiangsu Province, China. The field consisted of a widely cultivated rice variety with
 224 planting scheme of 3-5 seedlings per hole and 30×12 cm spacing between plants. The
 225 imaging was performed using random viewing angles at objective distances of ~60
 226 cm towards the rice plant using a Canon EOS 70D camera with resolutions of
 227 4032×3024 pixels. The images contain various numbers of small-sized panicles
 228 ranging from 50-90 per image, which have shown the complex interaction
 229 relationship between different rice plants. As shown in Figure 4, there were 141
 230 images and 126 images acquired under normal (9:00 am) and strong (2:00 pm)
 231 illumination conditions respectively. The picture of the rice panicle appears in yellow
 232 color, and the full image is filled with large number of light greenish rice leaves
 233 together with shadows due to the oblique illumination angle and partially due to the
 234 leaf occlusions. The average dimensions (length × width) of panicles in the image

data is about 260×180 pixels after selecting 200 independent panicles randomly and calculating the average size (length \times width) of their minimum circumscribed rectangles.

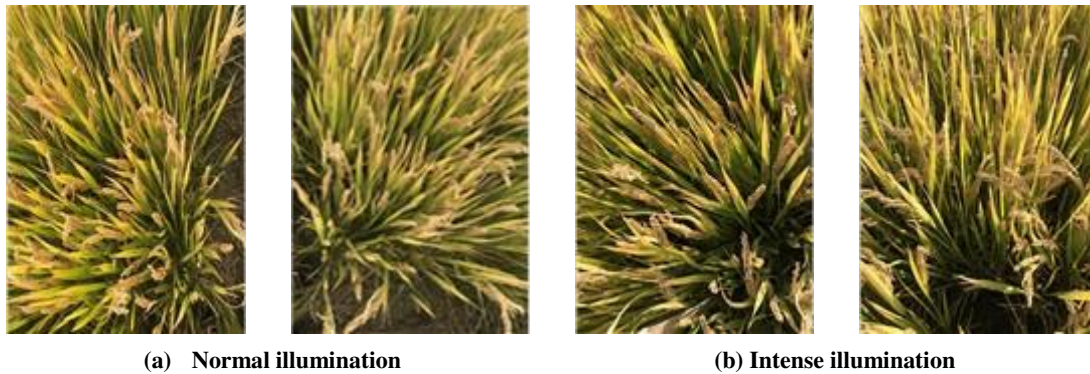


Fig. 4 Sample of have been taken under different viewing angles and illumination conditions

3.2 Multi-scale hybrid window dataset construction

3.2.1 Calculate the structure of the MHW

The average size of rice panicle in the data set is about 260×180 pixels which is less than one-tenth of the image size with occupancy about 0.4% of the full picture. This gives the most appropriate dimensions of the input images ranging between 260×180 pixels and 2600×1800 pixels as according to equation 4. As mentioned in section 2.2.1, the VGG16 network has been chosen because it is more effective to learn the features of objects particularly those with physical dimensions like that in our data set. The optimal dimensions of each layer of the multi-scale hybrid window can be assessed through equation 5, which gives the topmost 3 layers to be ideally having 2016×1512 pixels, 1008×756 pixels and 504×378 pixels respectively. Although theoretically the more of the network layers the richer that the features can be learned, however, it is a balance between performance and computational

complexity. When the layer with input images of sizes 504×378 pixels, it contains utmost only a few rice panicles which may not be economical in view of the amount of the extra computational and labeling workload involved. Hence, only the two extra topmost layers have been utilized in this work.

3.2.2 Formation of the MHW dataset

Among the 267 rice pictures collected, 130 of those (~50%) were randomly selected as the training set, and 57 pictures (~20%) were used as the validation set and the remaining 80 pictures (~30%) was used as the test data set. There is no data overlap among the training, validation and test sets. For the model training, we only construct the MHW dataset for the training set and the validation set. Conventional subsampling using a fixed scheme for altering image dimensions (Ghiasi et al., 2016) may not be desirable when the problem in question consists of targets in various sizes. Here, for each image in the training and validation data set, the raw image at 4032×3024 pixels resolution (hereafter referred as R1) is divided along the length and width in 4 and 2 equal parts respectively to form a four and sixteen units of sub-images respectively. Then these 4 sub-images at 2016×1512 pixels resolution (hereafter referred as R2), and 16 at 1008×756 pixels resolution (hereafter referred as R3) together with the raw image are collectively termed as multi-scale hybrid windows (MHW). Alternative MHW partition schemes which select different layers to train the model (such as R1 & R2, R2 & R3) have also been utilized in the experiment.

272 3.2.3 Target labeling schemes

273 The labeling of MHW images for training and validation dataset has been
274 performed manually by recording the coordinates of the minimum circumscribed
275 rectangle of the panicle, using the annotation software named 'LabelImg'. In the case
276 of panicles that have been partitioned into several parts, all parts are labeled as
277 independent rice panicles. In the case of the rice panicles that are occluded by leaves,
278 only the exposed parts are labeled as independent panicles. For panicles that are
279 overlapping to each other, the front panicles are labeled as independent target while
280 the rear part will be marked only if they are visible. Figure 5 shows some examples of
281 annotation schemes that have been adopted in this work.

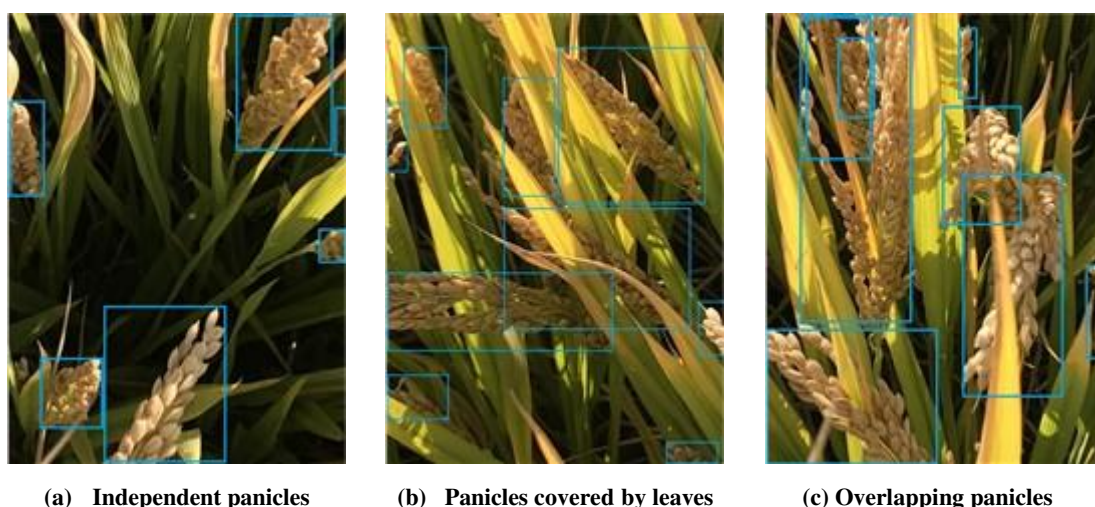


Fig. 5 Examples of manual annotations of panicles

282 3.3 Configuration of test dataset for experiments

283 The remaining 80 raw pictures at resolution of 4032×3024 pixels (i.e. at 'R1') in
284 the section 3.2.2 was termed as the 'Dataset_test' in this paper. Each image in the
285 Dataset_test was then partitioned equally into 16 sub-images giving a total of 1280
286 pictures at 1008×756 pixels (i.e. at 'R3'), which is collectively referred as

287 ‘Dataset_test_1’. The number of panicles in the picture of Dataset_test_1 ranges from
 288 0-20. By merging two of the adjacent neighboring sub-images of the 16 partitioned
 289 images of the raw pictures produces 4×80 of new images at resolution of 2016×1512
 290 (i.e. at ‘R2’). All these sub-images were then sorted into another two data sets
 291 (Dataset_test_2 and Dataset_test_3) as according to the number of panicles in the
 292 imagery as illustrated in Table 3. These 3 data sets provide a range of different
 293 number (and hence different sizes) of panicles as targets for the classifiers to detect
 294 (and count) under various degrees of background cluttering.

295 Images of rice panicles collected in real fields are normally exhibit blurring and
 296 discoloring due to the complicated environment in the rice field. Imaging such
 297 complex scene by using limited depth of view optical systems under various
 298 illumination geometries, will result in some objects that are out-of-focus and/or
 299 discolored due to the variable irradiance and also targets at various depth across the
 300 scene. As mentioned image data had been collected at two different solar irradiances:
 301 one at 9 am (thereafter referred as ‘normal’ illumination) and also at 2 pm (thereafter
 302 referred as ‘intense’ illumination). Another data set, termed as the ‘Dataset_test_4’
 303 which is organized in four categories of a) in-focus & normal illumination, b) in-focus
 304 & intense illumination, c) blurry & normal illumination and d) blurry & intense
 305 illumination.

306 **Table 3. Description of the datasets that have been employed in this study**

Name of the Datasets	Composition of Dataset		
	Category	Size of Image Pictures in Dataset	Number of Pictures in Dataset

Dataset_test	Original test images	4032×3024	80
Dataset_test_1	Cut in 16 equal parts	1008×756	1280
Dataset_test_2	0~10(panicle number in sub-window image)	1008×756	205
	11~20(panicle number in sub-window image)	1008×756	108
	21~30(panicle number in sub-window image)	1008×1512	70
	31~40(panicle number in sub-window image)	1008×1512	41
Dataset_test_3	41~50(panicle number in image)	4032×3024	22
	51~60(panicle number in image)	4032×3024	22
	61~70(panicle number in image)	4032×3024	16
	71~80(panicle number in image)	4032×3024	9
	81~90(panicle number in image)	4032×3024	7
Dataset_test_4	In-focused & Normal illumination	1008×756	67
	In-focused & Intense illumination	1008×756	72
	Blurry & Normal illumination	1008×756	62
	Blurry & Intense illumination	1008×756	74

307 3.4 Construct the automatic rice panicle counting model

308 3.4.1 Computational hardware and platform

309 All processing performed in this work was carried out by the AMAX's PSC-
310 HB1X deep learning workstation which consisted of an Intel(R) E5-2600 v3 CPU
311 with clock speed of 2.1GHZ, 128GB DRAM, 1TB hard disk and with a GeForce
312 GTX Titan X graphics card. The operating environment was Ubuntu 16.0.4, Caffe,
313 Python 2.7.

314 3.4.2 Model training

315 The proposed MHW-PD network consists of three parts: the feature learning
316 network, the candidate region generation network and the detection network (Figure
317 6). The feature learning network utilizes the VGG16 network but without its
318 classification layer. The region generation network traverses the feature map
319 (stride=1) with a 3×3 convolution kernel and a 9 candidate region with three aspect
320 ratios of 1:1, 2:1 and 1:2 to indicate the high probability of target (panicle) presence is

321 generated by the proposal layer. The detection network uses a convolution operation
 322 with a convolution kernel size of 1×1 and a sliding step size of 1 to achieve full
 323 connectivity.

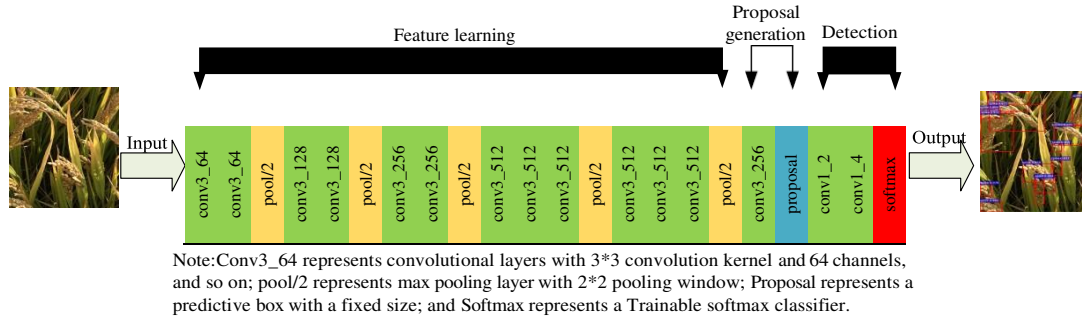


Fig. 6 Schematic Structural configuration of the proposed MHW-PD network

324 The VGG16 network is trained through the optimization of the loss function
 325 using the stochastic gradient descent (SGD) method for the identification of panicles,
 326 and the location of the targets are obtained through the regression model. We set the
 327 batch-size and iteration steps to 128 and 80000 respectively, and the learning rate
 328 changes from 0.001 to 0.0001 after iteration steps reaches 50000. The loss function
 329 consists of contributions from the classification and regression loss as shown in
 330 equation (6):

$$331 \quad (\{P\}, \{t\}) = \frac{1}{N_{cls}} \sum_i L_i^{cls} + \lambda \frac{1}{N_{reg}} \sum_i P_i^* L_i^{reg} \quad (6)$$

332 Where the N_{cls} represents the mini-batch size of training, N_{reg} represents the
 333 generated number of candidate regions, i is the anchor number, the weighting
 334 parameter λ is set as $\lambda=10$. The P_i is the probability of the anchor point being as
 335 target, and when the anchor point is predicted as positive the corresponding P_i^*
 336 value is given as 1 and otherwise it is 0 if the anchor is negative. t_i and t_i^*
 337 represent the coordinates of the upper left and lower right vertex of the predicted

338 bouncing box respectively. L_{cls} and L_{reg} are the logarithmic and robust regression

339 loss respectively:

$$340 \quad L_{cls}(P_i, P^*) = -\log [P^* P + (1 - P^*)(1 - P)]$$

(1)

$$341 \quad L_{reg}(t_i, t_i^*) = \begin{cases} 0.5(t_i - t_i^*)^2 & |t_i - t_i^*| < 1 \\ |t_i - t_i^*| - 0.5 & |t_i - t_i^*| \geq 1 \end{cases} \quad (8)$$

342 3.5 Performance assessment indexes

343 The counting accuracy and the false detection rate have been utilized as the
 344 performance indexes in this work. The counting accuracy (P_c) refers to the ratio of
 345 detecting the correct number of panicles to the actual number of panicles; while the
 346 false detection rate (P_e) is the ratio of the detection error (false positive) to the actual
 347 number of panicles (ground truth) in the imagery data set:

$$348 \quad P_c = N_{cor}/N_{real} \quad (9)$$

$$349 \quad P_e = N_{err}/N_{real} \quad (10)$$

350 Where N_{cor} and N_{err} are the correct (true positive) and wrong (false positive)
 351 number of panicles detected by the model respectively, and N_{real} represents the
 352 actual number of panicles in the test sample.

353 Prior to the accuracy assessment, the repeated counting of the same panicle from
 354 the MHW partitioned pictures is firstly evaluated. This is achieved through the
 355 assessment of the repetition ratio (P_{rep}) as shown in the equations (11), (12) and (13):

$$356 \quad P_{rep} = \frac{N_{rep}}{\sum^k N} \quad (11)$$

$$357 \quad N_{rep} = \sum^k_{i=1} N_{subi} - N_{cor} \quad (12)$$

$$i = 1$$

$$P_{rrep} = \frac{\sum_{i=1}^k N_{subi} - N_{rep}}{N_{terp}} \quad (13)$$

where N_{rep} represents the number of the repeated panicles that has been removed by the fusion algorithm; N_{subi} is number of the detected panicle in the i^{th} sub-window; k is the total number of the sub-windows in the picture; N_{cor} represents the number of panicles detected after image fusion; P_{rrep} is the de-duplication rate and N_{terp} is the number of the panicles that have been counted repeatedly.

4 Results

4.1 Parameters that affect the performances of classifier

Based on the hardware mentioned in section 3.4.1, it cost about 0.102s to test a sub image for our model. In addition, to testify how the performance of the classifier is affected by the receptive field of the network, the number of layers in the hybrid windows and the effectiveness of the proposed MHW image partitioning method, two different ways of sample preparations have been utilized:

A . MHW partitioning method (see section 3.2)

B . Down-sampling method (DS):

a. Each image in the training and validation data sets (i.e. the Dataset_test) is down-sampled by a factor of 2 from the raw resolution of R1 into R2, which is then down-sampled again into R3. The down sampling was done through Laplacian filtering method (Ghiasi et al., 2016).

b. This method does not exploit any window partitioning.

The experiment was performed using one to three layers of the MHW, two

different networks (ZF and VGG16) which had receptive fields to target size ratio (S_{RF}/S_{obj}) of 0.4 and 0.96 respectively (see Table 1), and data prepared with (i.e. the MHW method) and without window partitioning processing (i.e. the DS method). The averaged counting accuracy P_c over 3 experimental runs using pictures of dataset_test_1 is shown in Table 4.

Table 4. Average panicle detection results under various network configurations

Number of MHW layers	Resolution of MHW layer	$P_c/\%$ (Average \pm STD)			
		Down sampling (DS)		MHW	
		ZF	VGG16	ZF	VGG16
1	4032×3024	31.0% \pm 0.37%	34.7% \pm 0.37%	37.4% \pm 1.12%	38.1% \pm 0.56%
1	2016×1512	38.7% \pm 0.96%	42.3% \pm 0.37%	45.2% \pm 0.37%	47.7% \pm 0.56%
1	1008×756	50.2% \pm 0.55%	53.5% \pm 0.56%	58.4% \pm 0.37%	61.2% \pm 0.56%
2	4032×3024	41.6% \pm 1.10%	44.7% \pm 1.12%	47.9% \pm 0.56%	50.2% \pm 0.55%
2	2016×1512	53.5% \pm 0.56%	56.5% \pm 1.17%	63.0% \pm 0.92%	66.7% \pm 0.56%
2	1008×756	63.5% \pm 0.73%	72.9% \pm 0.92%	73.1% \pm 0.76%	78.1% \pm 0.73%
3	4032×3024	74.8% \pm 0.37%	78.5% \pm 0.36%	83.3% \pm 0.92%	87.2% \pm 0.37%
	2016×1512				
	1008×756				

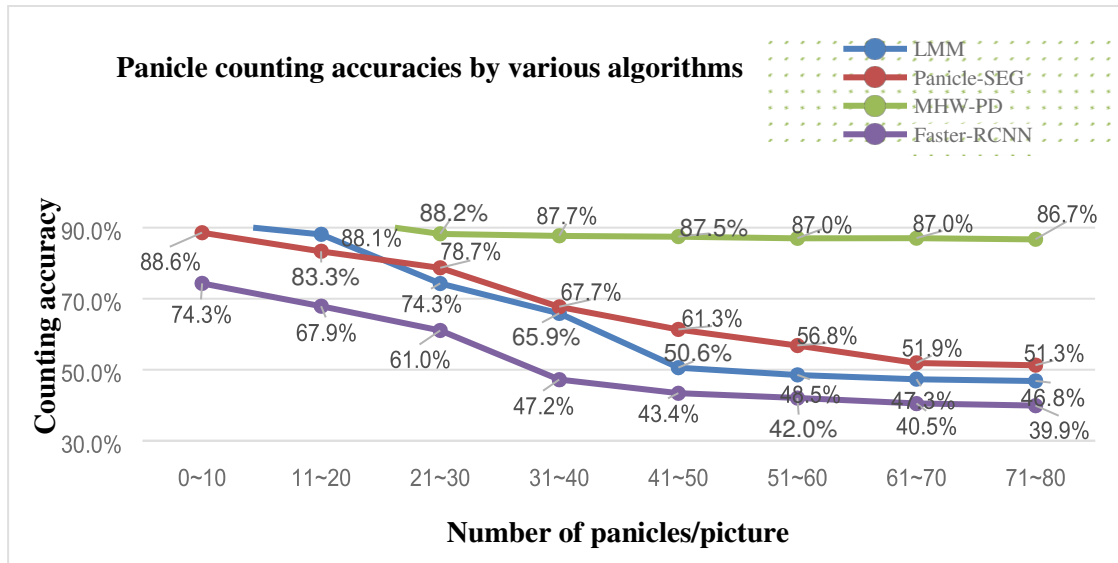
Firstly, it is noted that the reduction of the layer resolution from R1 (4032×3024 pixels) to R3 (1008×756 pixels), e.g. when the single layer of MHW of the VGG16 network is used, the panicle counting accuracy is increased from 38.1% to 61.2%. This is an almost 60% better detection when the layer is in lower (i.e. at R3) resolution. This trend of enhancement in panicle counting accuracy is seen regardless whether the data set was prepared with or without window partitioning. Secondly, the detection performance by the VGG16 network is ~5% better than that of the ZF network. This apparent small difference observed from the well matched receptive

field of the VGG16 comparing to the very mismatched ZF network, is mainly due to the mixture of panicle densities in the current employed dataset_test_1. The proposed MHW enhances more of detection accuracy when the target sizes are small, i.e. when the densities of panicles are high (see section 4.2). Thirdly, when the image partitioning technique is applied (i.e. the MHW method) there is 14.4% increase in the counting accuracy in comparison to the detection that performed using non-image partitioning technique (i.e. the DS method). This can be seen, e.g. from the 61.2% accuracy given by the single layer of MHW of the VGG16 that uses input data at R3 resolution, in direct comparison to that of 53.5% obtained from the down-sampling (DS) method. Note that this ~14% of performance enhancement by using MHW is not a representative figure because of the mixed panicle densities in the dataset_test_1 that has been employed in this experiment. Fourthly, it is well-known that the increasing number of the MWH layers improves the detection performance in general, which can be seen from Table 4 that there is over 40% increase of panicle counting accuracy when the number of layers is increased from 1 to 3. Despite of using the image data set (i.e. the dataset_test_1) that contains a mixture of different panicle densities, the results presented in this section indicate that the use of multi-scale hybrid windows enhances the feature learning capacity of the network, particularly when the target sizes in the imagery is closely match to the receptive field of the feature extraction network.

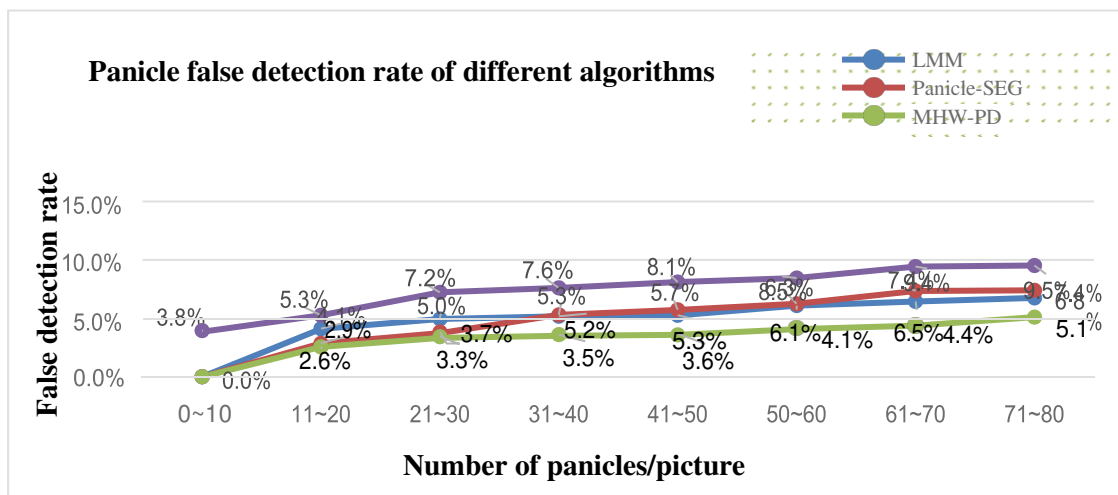
413 4.2 Effectiveness of MHW-PD for the detection of large number of panicles

414 Followed by the positive results given by the previous section, the experiment
415 here is aimed at assessing how effective is the proposed MHW-PD for the
416 identification of different number (i.e. density) of rice panicles of the scene which is
417 presented by the input imagery data. This section examines the proposed method
418 vigorously by assessing the ability of the proposed MHW-PD method for counting
419 high number of panicles (i.e. small target size), and, to compare its performance with
420 respected to various existing algorithms. Three competing methods: a) the technique
421 that based upon filtering using Laplacian, Median and Maxima (LMM)
422 filters(Fernandez-Gallego et al., 2018); b) the Panicle-Seg(Xiong et al., 2017) which
423 segments rice panicles (i.e. identification) using super-pixel clustering and CNN
424 classification and c) the Faster-RCNN that performs panicles detection without any
425 window partitions; had been utilized here to verify the usefulness of the proposed
426 MHW technique for enhancing the extraction of features particularly those from small
427 targets. Both Dataset_test_2 and Dataset_test_3 had been used as the test data for all
428 classifiers employed in this experiment. All competing classifiers had been trained
429 using the 130 pictures of the training data set which were in R1 resolution (i.e.
430 4032×3024 pixels), while the proposed MHW-PD was trained using the partitioned
431 images in 3 different scales as described in section 4.4.1. All experiments were based
432 on the VGG16 and they were repeated 3 times. The abilities in terms of the averaged
433 counting accuracies and error detection rates of all classifiers to cope with scenes (i.e.

images) which contain various numbers of panicles are plotted in Figure 7.



(a) The Counting accuracy of the MHW-PD and together with other competing algorithms as a function of number of panicle/picture



(b) The false detection rate of the MHW-PD and the other competing algorithms as a function of number of panicle/picture

Fig. 7 The Detection results of the MHW-PD and together with other competing algorithms to demonstrate the effectiveness of the proposed method particularly when high numbers of panicles are present in the scene

Figure 7 displays a rather astonished picture which exhibits the robustness of the classifiers to the increasing complexity of the rice field conditions vividly. At a glance there are two rather distinct trends that can be observed: one is the rapid decreasing detection performance, in the order of ~40%, when the number of panicles is

increased from ~10 to ~50 in the scene. The other obvious trend is the very robust detection performance, with a slight drop of ~8% even when the panicle number in the scene is increased to 70-80/picture. The latter result is given by the proposed MHW-PD method which utilizes a pre-processing technique with the classification unit invariant to other competing methods (e.g. the Faster-RCNN).

One point to note is the direct comparison between the performances of the proposed MHW-PD with respected to the Faster-RCNN: in both cases the processing networks are essentially the same, however, the panicle classification performances between these two seemingly the same network are completely different. The averaged detection accuracies given by the Faster-RCNN and the MHW-PD for the scenes with panicle number <40 (i.e. when the target sizes are much larger than 260×180 pixels) are 62.6% and 90.8% respectively. This is almost 45% better detection by the MHW-PD when the panicle sizes are relatively large. However, the same two techniques for classifying the scenes with panicle number between 40 and 80 give the averaged accuracies of 41% and 87% respectively. This is over 110% of better detection by the proposed MHW-PD when the panicle sizes are small (i.e. smaller than the average size of 260×180 pixels).

Figure 8 depicts representative classified images of the rice panicle scenes obtained by using the proposed MHW-PD method. The wide range of target sizes, as depicted by the huge variations of areas of the bounding boxes from large in Figure 8(a) to very small in Figure 8(e), highlights the increasing complexity of the scene

460 which induces higher clutter background and the increasing difficulties to extract the
 461 feature of small targets faithfully as that depicted in Figure 8(d) & (e). This result may
 462 give another evidence that the detection capability of the propose MHW-PD method
 463 is robust against high number (density) of panicles in the rice field.

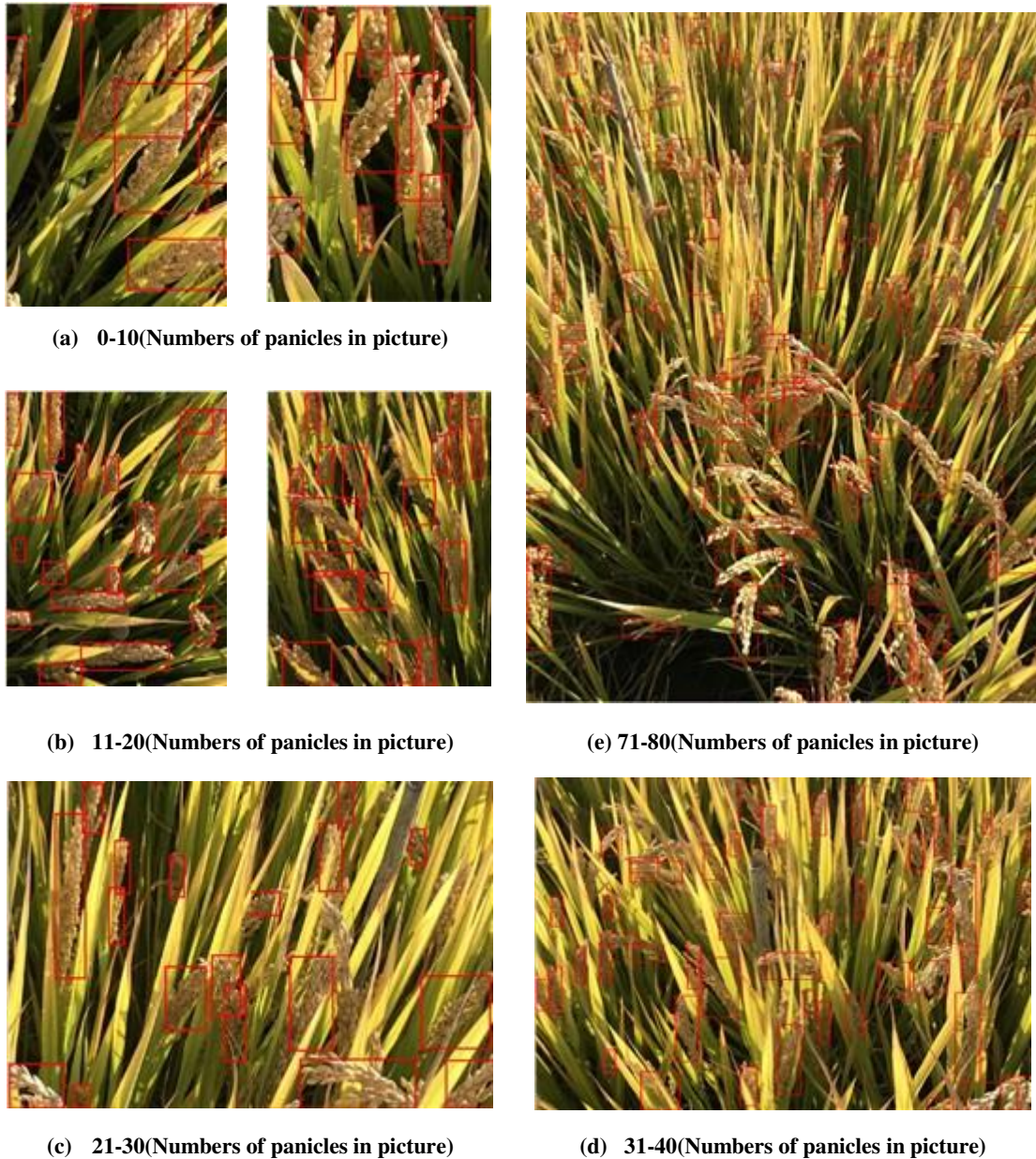


Fig. 8 Sample of pictures to illustrate the effectiveness of the proposed MHW-PD for the detection of various sizes of panicles in the scene

464 4. 3 Robustness of MHW-PD against numbers of panicles in the scene

465 This section highlights how the proposed MHW-PD enhances the detection of

466 small target in the imagery data over the conventional classification routine. Here, the
 467 ‘small’ target in this work is referred to the relative size (in pixel unit) of the target
 468 object with respected to the pixel dimension of the input images. Figure 9a illustrates
 469 the typical classification result produced by the classifier (Faster-RCNN) in which the
 470 dimension of the input test image is at R1 resolution (i.e. 4032×3024 pixels). It is seen
 471 that some small panicles have been missed out in this classification result. The
 472 classification of the same test image after it is partitioned into 4 sub-windows (at R3
 473 resolution) exhibits much better detections as it is illustrated in Figure 9b. After the
 474 removal of duplicated counts of dissected panicles at the boundary of sub-windows
 475 through the fusion algorithm, the end result as depicted in Figure 9c shows much
 476 better detection than that of Figure 9a. At a glance over Figure 9a and Figure 9c, one
 477 may notice immediately the distinct difference of the sizes of the panicle bouncing
 478 boxes between these two figures: more small bouncing boxes can be spotted from the
 479 MHW-PD result (Figure 9c).



(a) Result without cutting

(b) Results of HW after cutting

(c) Result after fusing

Fig. 9 Demonstrate the effectiveness of the MHW-PD system

480 Since the sub-window fusion plays an essential part in the overall performance of
 481 the MHW-PD, the robustness of the fusion algorithm over increasing complexity of
 482 the scene was investigated here. The experiment was designed to evaluate the
 483 detection performance of the algorithm for a range of assorted number of panicles in
 484 the data set (Dataset_test_3). The repetition ratio (P_{rep}) is to measure the probability
 485 of panicles being counted repeatedly, while the de-duplication rate (P_{rrep}) represents
 486 the ability of the fusion algorithm to remove the repeated counts. It can be seen from
 487 Figure 10 that P_{rep} is rather constant in the medium density (number) of panicles
 488 and it increases slightly at high number of targets in the scene. The P_{rrep} also
 489 exhibits rather steady performance at ~95% removal rate when the panicle number
 490 <90, but it tends to decrease slightly to ~92% at high end of >100 panicles in the
 491 scene. This result may give another support towards the robustness of the proposed
 492 MHW-PD system.

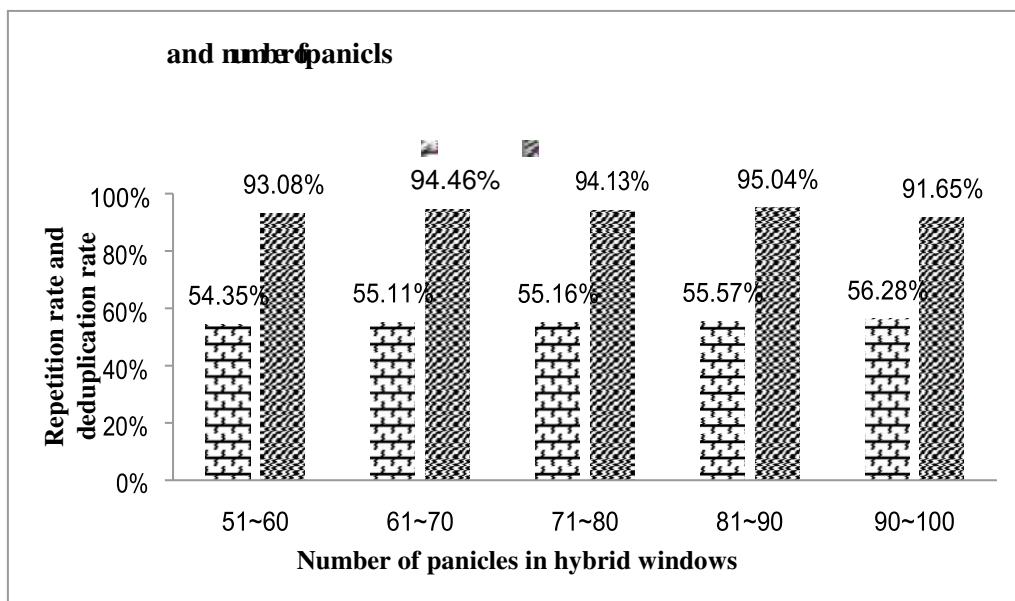


Fig. 10 Highlight the robustness of the P_{rep} and P_{rrep} of the MHW-PD against the number of panicles

4. 4 Robustness of MHW-PD against illumination and imaging artefacts

As shown in figure 8(e), it is observed that the detection results in the top of this image are obviously worsen than the bottom part. During the course of this work, we found that the bottom of images were sharp (in-focused) while the top part were blurry and fuzzy. To understand the robustness of our counting model when the quality of the input images was subjected to various degree of blurriness and shadowing artefacts, the Dataset_test_4 had been used as the test data (see Table 3), which consisted of field images subjected to various degree of blurriness and shadowing and taken under normal (i.e. weak shadowing) and intense (i.e. strong shadowing) illumination conditions. The number of panicles per picture in the Dataset_test_4 was <20. The experiments were run 3 times based on VGG16 to obtain the mean detection accuracy and the associated standard deviation errors. Typical images of the classification outputs from the MHW-PD for the detection of panicles from the dataset_test_4 which contains blurry and strong shadowing pictures are shown in Figure 11. The average counting accuracies and the average false detection rates for the panicle detections of this data set are tabulated in Table 5, which reveals that the hard shadowing imposed by the intense illumination does not affect the detection efficiency significantly. However, there is ~24% drop of detection when the input images for testing are blurry. This may indicate that the fuzziness of the input image does affect the extraction of textural features as expected.

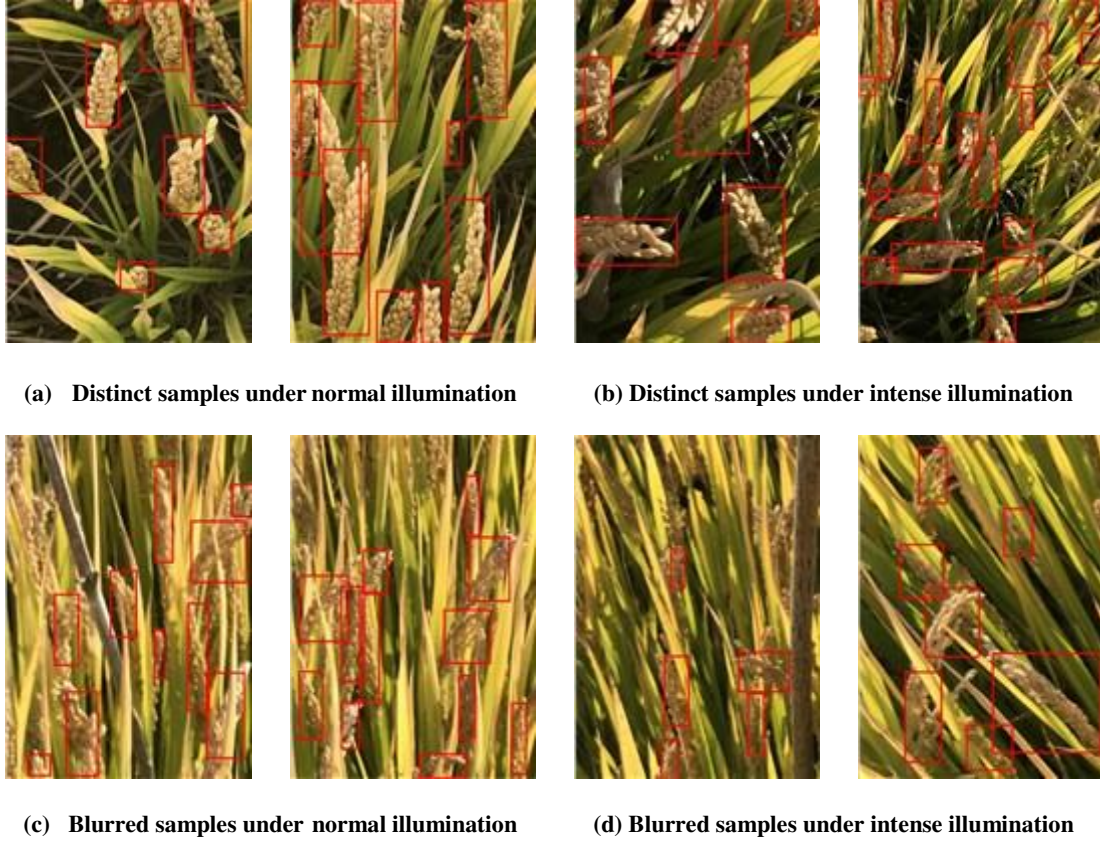


Fig. 11 To illustrate the Detection of panicles under various illumination and imaging conditions

Table 5. Average detection accuracies for images taken under various illumination and imaging conditions

Quality of input image data	Illumination conditions	$P_d/\%$ (Average \pm STD)	$P_e/\%$ (Average \pm STD)
In-focused pictures	Normal (weak) illumination	94.5% \pm 0.78%	1.6% \pm 0.26%
	Intense (strong) illumination	92.4% \pm 0.37%	2.0% \pm 0.16%
	Mixture of Normal & Intense illumination	93.4% \pm 0.51%	1.8% \pm 0.07%
Blurry pictures	Normal (weak) illumination	70.1% \pm 0.89%	3.3% \pm 0.42%
	Intense (strong) illumination	68.5% \pm 1.08%	3.5% \pm 0.34%
	Mixture of Normal & Intense illumination	69.3% \pm 0.46%	3.4% \pm 0.27%

5 Discussions

This work has reported a method (MHW-PD) to count the in-field small-sized rice panicle and function robustly independent of the panicle density. Based on the results given by the series of experiments, it is suggested that the dynamic strategies for network selection multi-scale hybrid windows construction tend to enhance the

feature learning capacity of the small-sized panicles and eliminate the impact of the increase in the number of rice panicles. Compared to the pure counting method based on thermal imagery (Fernandez et al., 2019), it should be noted that, the individual rice panicle images can be segmented easily since their positions are predicted by MHW-PD. It means more phenotypic traits can be analyzed further in detail, such as the length of panicle, the radian of panicle, the number of panicle grains, the disease spot or the saturation of panicle grains and so on. In addition, the result of 87% is an average accuracy of different clarities, illuminations, occlusions and panicle numbers per image. While most of the current phenotypic studies focus on indoor potted rice, which means more stable imaging conditions (no fuzzy panicles), fewer panicles and less occlusion in the image. Thus, we suppose the MHW-PD can meet the needs of phenotypic researchers to some extent for mining the relationship from traits to genotypes, while there are also some limitations and practical issues we have to consider when the MHW-PD applied in real situations, which may constitute research directions that will be pursued in the future work.

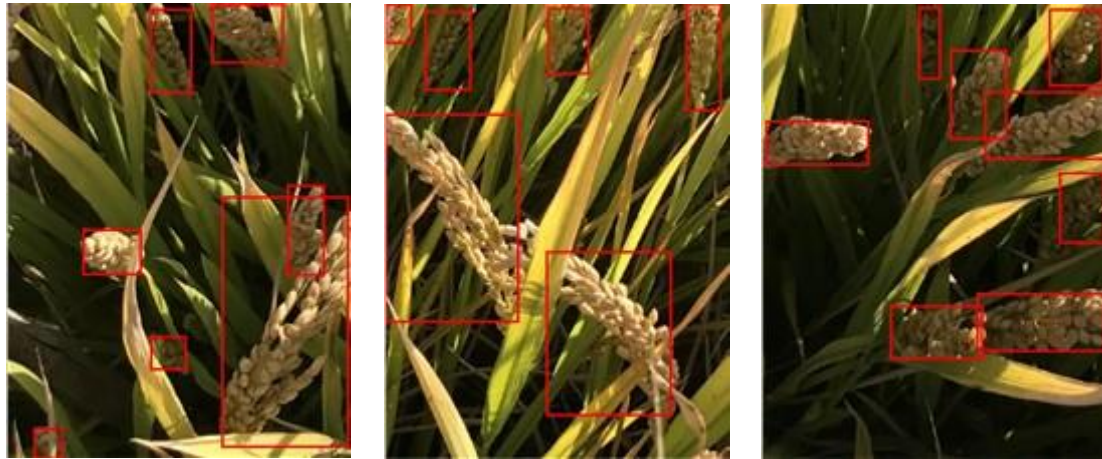
(1) MHW-PD against occlusions. Occlusion has been one of the main factors that affect the performance of panicle counting, which may come from the high plant density and drooping, particularly when the assessment method is based on image recognition technology. In this section, 3 different kinds of occlusions have been studied: a) independent panicle when there is no obstruction, b) occlusion by leaf and c) overlapping panicles. The data set that been utilized in this experiment consisted of

540 <20 panicles/picture and the training/testing conditions of the MHW-PD network
 541 were the same as the previous experiments. Sample pictures of detection results for
 542 the identification of panicles in the data set that consists of these 3 types of occlusions
 543 are shown in Figure 12, and their averaged detection accuracies are tabulated in table
 544 6. The result has shown quite clear that the detection is strongly affected by
 545 occlusions which causes some ~30% degradation of panicle accuracies with respected
 546 to the unobstructed base line, when the target panicle is occluded by leaves. Worse
 547 still is a ~60% drop in the detection accuracy when panicles in the scene are self-
 548 occluded. This large drop in detection efficiency is the inability of the classifier to
 549 discriminate the overlapped panicles and in most cases, it misclassifies the
 550 agglomerated entity as one panicle (see Figure 12b). The occlusion by leaves is not as
 551 severe as that of the self-occlusion as long as the panicle sizes are relatively larger
 552 than the leaf blades. However, the detection is seen worse when small panicles are
 553 occluded by the leaves or when large part of the panicles are covered by leaves (see
 554 Figure 12c). The very limited amount of features is not sufficient enough for the
 555 classifier to discriminate the leaf and panicle.

556 **Table 6. Results of images with different occlusions**

Types of Occlusions	P_d %	P_c %
Independent panicles (114 images)	95.5%	1.2%
Panicles partially covered by leaves (52 images)	62.8%	6.3%
overlapping panicles (46 images)	37.8%	29.4%

557



(a) Detect results of independent panicles



(b) Detect results of overlapping panicles



(c) Detect results of panicles covered by leaves

Fig. 12 Illustrate the detection by the MHW-PD for the panicles that are subjected to various occlusions

558 (2) MHW-PD against different imaging heights. Panicle size is the most important
 559 factor to consider when we designed the MWH-PD. However, when it comes to the
 560 different imaging heights, the main effect is the change of average panicle size. For

example, if the images taken at a higher/lower altitude, the number of panicles will rise/fall sharply while the panicle size become smaller/bigger in the single image. Our ideal is selecting feature learning network which can effectively perceive a complete panicle and constructing the multi-scale hybrid windows which can extract the multi-scale panicle features. Therefore, in order to ensure the application effect of the MHW-PD, we have to design different reasonable image acquisition schemes (viewing angles, depth of field, focusing ability and optical aberrations et al.) for different particular imaging heights, which can ensure the panicle size is enough to find a matching feature learning network. At this time, the gap caused by different heights can be filled easily by selecting suitable network and constructing suitable MHW. However, we do not mean the MHW-PD can be applied under any heights because the sizes of the reception fields of the existing network are limited. From this angle, there may be a possibility to extend MHW-PD from the camera images to the high-resolution UAV images in theory, but more issues need to deal with to realize the application. For example, the huge amount of labeling work and some new processing mechanisms for the blur of panicles caused by the propeller wind when the UAV flew at a very low altitude.

(3) MHW-PD against different rice varieties. The shape of panicles has great influence on detection accuracy, which not only comes from the panicles of different rice varieties, but also from the panicles of same variety during different growth periods. In order to realize large-scale promotion application, we have to solve this

582 inevitable problem, while it is very different to construct a universal model. Firstly,
583 collecting images of all rice varieties/growth periods and labeling them costs a lot of
584 money and time. Secondly, universal model means we need count and identify the
585 species at same time. For deep learning networks, the great difficulty to solve this
586 problem lies in how we can realize the feature representation of several rice varieties,
587 which have small difference and even some of the difference is only local. The
588 features can not only represent the rice panicles but also have enough differentiation
589 to support the effective fine-grained classification for those different subspecies and
590 varieties of rice. The problem may become even more difficult for the field scenarios
591 because of the interference of complex field noise. One possible solution we now
592 have tried is to iteratively build single model for every variety or growth period and
593 cascade a multi-discrimination model for counting and identifying.

594 **6 Conclusions**

595 Counting small-sized rice panicles efficiently and accurately by using image based
596 technique has been a challenging task. This paper proposes a new, yet simple method
597 termed as MHW-PD to realize the efficacy of rice panicle counting especially when
598 high number (density) of small-sized rice panicles is involved. The main contribution
599 of this work is to introduce a multi-scale hybrid window (MHW) pre-processing 600
technique for enhancing the richness of the target feature, and then to maximize the 601 feature
extraction efficiency of the network through matching the target sizes with the 602 receptive
field of the network. Through experimental design and result analysis, the

603 conclusions can be summarized as follows:

604 (1) The proposed MHW-PD can significantly improve the counting accuracy for the 605
scene where large numbers of panicles in a signal image. The combined effects of
606 selecting the appropriate feature learning network and constructing the optimal 607
hybrid window shown that the average counting accuracy of MHW-PD is 87.2%,
608 which achieves >110% of detection efficiency better than that of the Faster- 609
RCNN for the dense scenes whose number of panicles is between 50 and 80 per 610
image.

611 (2) The MHW-PD has better stability in counting accuracy for the increasing number 612
of panicle. When the panicle number increases from 10 to 80, the counting 613
accuracy of MHW-PD comes down by 7.6%.

614 (3) The proposed MHW-PD can be used for infield scenes with hard shadowing 615
imposed by intensified illumination, while the imaging and occlusion artefacts 616
will affect the detection efficiency significantly. There is ~24% drop of detection
617 when the input images for testing are blurry. When the panicles occluded by 618
leaves and self-occluded with panicles crossing each other, the counting accuracy
619 is ~30% and ~60% degradation respected to the unobstructed base line.

620 **Acknowledgements**

621 This paper is supported in part by the National Natural Science Foundation of 622
China (No. 31872847); the Key Program of Science and Technology Infrastructure of 623
Jiangsu Province of China (Modern Agriculture, BE2019383).

624 REFERENCES

625 Aich S, Stavness I. Leaf counting with deep convolutional and deconvolutional 626
networks. In: Proceedings of the IEEE International Conference on Computer Vision, 627
2017, pp. 2080-2089.

628 Alkhudaydi T, Zhou J. SpikeletFCN: Counting Spikelets from Infield Wheat Crop 629
Images Using Fully Convolutional Networks. In: International Conference on 630
Artificial Intelligence and Soft Computing, 2019, pp. 3-13, Springer.

631 Barré P, Stöver BC, Müller KF, Steinhage V. LeafNet: A computer vision system for 632
automatic plant species identification. *Ecological Informatics*, 40(2017), pp. 50-56, 633
10.1016/j.ecoinf.2017.05.005

634 Cointault F, Guerin D, Guillemain JP, Chopinet B. In-field *Triticum aestivum* ear 635
counting using colour-texture image analysis. *New Zealand Journal of Crop and 636
Horticultural Science*, 36(2008), pp. 117-130, Doi 10.1080/01140670809510227

637 Dobrescu A, Valerio Giuffrida M, Tsaftaris SA. Leveraging multiple datasets for deep 638
leaf counting. In: Proceedings of the IEEE International Conference on Computer 639 Vision,
2017, pp. 2072-2079.

640 Du Y, Cai Y, Tan C, Li Z, Yang G, Feng H, Dong H. Field wheat ears counting based 641
on superpixel segmentation method. *Scientia Agricultura Sinica*, 52(2019), pp. 21-33, 642
10.3864/j.issn.0578-1752.2019.01.003

643 Duan LF, Huang CL, Chen GX, Xiong LZ, Liu Q, Yang WN. Determination of rice 644
panicle numbers during heading by multi-angle imaging. *Crop Journal*, 3(2015), pp.

645 211-219, 10.1016/j.cj.2015.03.002

646 Fernandez-Gallego JA, Kefauver SC, Gutierrez NA, Nieto-Taladriz MT, Araus JL. 647
Wheat ear counting in-field conditions: high throughput and low-cost approach using 648 RGB
images. *Plant methods*, 14(2018), pp. 22-34, 10.1186/s13007-018-0289-4

649 Ferrante A, Cartelle J, Savin R, Slafer GA. Yield determination, interplay between 650
major components and yield stability in a traditional and a contemporary wheat across 651 a
wide range of environments. *Field Crops Research*, 203(2017), pp. 114-127, 652
10.1016/j.fcr.2016.12.028

653 Ghiasi G, Fowlkes CC. Laplacian pyramid reconstruction and refinement for semantic 654
segmentation. In: *European Conference on Computer Vision*, 2016, pp. 519-534, 655
Springer.

656 Girshick R. Fast r-cnn. In: *Proceedings of the IEEE international conference on* 657
computer vision, 2015, pp. 1440-1448.

658 Girshick R, Donahue J, Darrell T, Malik J. Rich feature hierarchies for accurate object 659
detection and semantic segmentation. In: *Proceedings of the IEEE conference on* 660
computer vision and pattern recognition, 2014, pp. 580-587.

661 Giuffrida MV, Minervini M, Tsafaris SA. Learning to count leaves in rosette plants. 662
In: *Proceedings of the Computer Vision Problems in Plant Phenotyping (CVPPP)*, 663
2016, pp. 1.1-1.13.

664 Guo W, Fukatsu T, Ninomiya S. Automated characterization of flowering dynamics 665
in rice using field-acquired time-series RGB images. *Plant methods*, 11(2015), pp. 7-

666 23, 10.1186/S13007-015-0047-9

667 Han J, Zhang D, Cheng G, Liu N, Xu D. Advanced deep-learning techniques for 668
salient and category-specific object detection: a survey. IEEE Signal Processing 669
Magazine, 35(2018), pp. 84-100, 10.1109/Msp.2017.2749125

670 Hasan MM, Chopin JP, Laga H, Miklavcic SJ. Detection and analysis of wheat spikes 671
using Convolutional Neural Networks. Plant methods, 14(2018), pp. 100-113, 672
10.1186/S13007-018-0366-8

673 He K, Zhang X, Ren S, Sun J. Spatial pyramid pooling in deep convolutional 674
networks for visual recognition. IEEE transactions on pattern analysis and machine 675
intelligence, 37(2015), pp. 1904-1916, 10.1109/TPAMI.2015.2389824

676 Jin XL, Liu SY, Baret F, Hemerle M, Comar A. Estimates of plant density of wheat 677
crops at emergence from very low altitude UAV imagery. Remote Sensing of 678
Environment, 198(2017), pp. 105-114, 10.1016/j.rse.2017.06.007

679 Krizhevsky A, Sutskever I, Hinton GE. Imagenet classification with deep 680
convolutional neural networks. In: Advances in neural information processing 681
systems, 2012, pp. 1097-1105.

682 Liu W, Anguelov D, Erhan D, Szegedy C, Reed S, Fu C-Y, Berg AC. Ssd: Single shot 683
multibox detector. In: European conference on computer vision, 2016, pp. 21-37, 684
Springer.

685 Lu H, Cao ZG, Xiao Y, Li YA, Zhu YJ. Region-based colour modelling for joint crop 686
and maize tassel segmentation. Biosystems Engineering, 147(2016), pp. 139-150,

687 10.1016/j.biosystemseng.2016.04.007

688 Madec S, Jin X, Lu H, De Solan B, Liu S, Duyme F, Heritier E, Baret F. Ear density 689
estimation from high resolution RGB imagery using deep learning technique. 690
Agricultural and forest meteorology, 264(2019), pp. 225-234,

691 10.1016/j.agrformet.2018.10.013

692 Maldonado Jr W, Barbosa JC. Automatic green fruit counting in orange trees using 693
digital images. Computers and electronics in agriculture, 127(2016), pp. 572-581, 694
10.1016/j.compag.2016.07.023

695 Mussadiq Z, Laszlo B, Helyes L, Gyuricza C. Evaluation and comparison of open 696
source program solutions for automatic seed counting on digital images. Computers 697 and
electronics in agriculture, 117(2015), pp. 194-199, 10.1016/j.compag.2015.08.010 698 Olsen
PA, Ramamurthy KN, Ribera J, Chen Y, Thompson AM, Luss R, Tuinstra M, 699 Abe N.
Detecting and Counting Panicles in Sorghum Images. In: 2018 IEEE 5th 700 International
Conference on Data Science and Advanced Analytics (DSAA), 2018, 701 pp. 400-409, IEEE.

702 Pound MP, Atkinson JA, Wells DM, Pridmore TP, French AP. Deep learning for 703
multi-task plant phenotyping. In: Proceedings of the IEEE International Conference 704 on
Computer Vision, 2017, pp. 2055-2063.

705 Qiongyan L, Cai J, Berger B, Okamoto M, Miklavcic SJ. Detecting spikes of wheat 706
plants using neural networks with Laws texture energy. Plant methods, 13(2017), pp. 707 83-
96, 10.1186/s13007-017-0231-1

708 Redmon J, Divvala S, Girshick R, Farhadi A. You only look once: Unified, real-time 709
object detection. In: Proceedings of the IEEE conference on computer vision and 710 pattern
recognition, 2016, pp. 779-788.

711 Redmon J, Farhadi A. YOLO9000: better, faster, stronger. In: Proceedings of the 712
IEEE conference on computer vision and pattern recognition, 2017, pp. 7263-7271.

713 Ren S, He K, Girshick R, Sun J. Faster r-cnn: Towards real-time object detection with 714
region proposal networks. In: Advances in neural information processing systems, 715 2015,
pp. 91-99.

716 Simonyan K, Zisserman A. Very deep convolutional networks for large-scale image 717
recognition. arXiv preprint arXiv:1409.1556, 2014),

718 Slafer GA, Savin R, Sadras VO. Coarse and fine regulation of wheat yield 719
components in response to genotype and environment. Field Crops Research, 720
157(2014), pp. 71-83, 10.1016/j.fcr.2013.12.004

721 Stein M, Bargoti S, Underwood J. Image Based Mango Fruit Detection, Localisation 722
and Yield Estimation Using Multiple View Geometry. Sensors, 16(2016), pp. 1915- 723 1923,
10.3390/S16111915

724 Szegedy C, Liu W, Jia Y, Sermanet P, Reed S, Anguelov D, Erhan D, Vanhoucke V, 725
Rabinovich A. Going deeper with convolutions. In: Proceedings of the IEEE 726
conference on computer vision and pattern recognition, 2015, pp. 1-9.

727 Xiong X, Duan L, Liu L, Tu H, Yang P, Wu D, Chen G, Xiong L, Yang W, Liu Q. 728
Panicle-SEG: a robust image segmentation method for rice panicles in the field based

729 on deep learning and superpixel optimization. *Plant methods*, 13(2017), pp. 104-119, 730

10.1186/s13007-017-0254-7

731 Zeiler MD, Fergus R. Visualizing and understanding convolutional networks. In: 732

European conference on computer vision, 2014, pp. 818-833, Springer.

733 Zhou C, Liang D, Yang X, Yang H, Yue J, Yang G. Wheat Ears Counting in Field 734

Conditions Based on Multi-Feature Optimization and TWSVM. *Frontiers in plant* 735

science, 9(2018), pp. 1024-1040, 10.3389/fpls.2018.01024

736

Declaration of interests

☐ The authors declare that they have no known competing financial interests or personal relationships that could have appeared to influence the work reported in this paper.

☐ The authors declare the following financial interests/personal relationships which may be considered as potential competing interests:

None

CRediT author statement

Xu can: Conceptualization, Methodology, Software, Data curation, Writing-Original draft preparation. **Jiang Haiyan:** Formal analysis, Supervision, Writing - Review & Editing, Funding acquisition. **Peter Yuen:** Writing - Review & Editing. **Zaki Ahmad Khan:** Validation Writing - Review & Editing. **Chen Yao:** Validation, Data curation.

MHW-PD: a robust rice panicles counting algorithm based on deep learning and multiscale hybrid window

Xu, Can

2020-04-15

Attribution-NonCommercial-NoDerivatives 4.0 International

Can X, Jiang H, Yuen P, et al., (2020) MHW-PD: a robust rice panicles counting algorithm based on deep learning and multiscale hybrid window. Computers and Electronics in Agriculture, Volume 173, June 2020, Article number 105375

<https://doi.org/10.1016/j.compag.2020.105375>

Downloaded from CERES Research Repository, Cranfield University